

# Coordinated Beating of Algal Flagella is Mediated by Basal Coupling

Kirsty Y. Wan and Raymond E. Goldstein

*Department of Applied Mathematics and Theoretical Physics,  
University of Cambridge, Wilberforce Road, Cambridge CB3 0WA, UK*

In a great many of the contexts in which groups of cilia or flagella are found they exhibit synchronized behavior. This includes phase-locking, as seen in *Chlamydomonas* flagella, and metachronal wave formation in the ciliary arrays of *Paramecium* or in the respiratory cilia of higher organisms. Since the observations by Gray and Rothschild of phase synchrony of nearby swimming spermatozoa, it has been a working hypothesis that synchrony arises from hydrodynamic interactions between beating filaments. Recent work on the dynamics of physically separated pairs of flagella isolated from the multicellular alga *Volvox* has shown that hydrodynamic coupling alone is sufficient to produce synchrony. Moreover, when the flagellar power strokes are oriented in the same direction they synchronize in-phase, but when opposed they synchronize in antiphase. The situation is more complex when considering multiple flagella on a single cell. Specifically, the unicellular biflagellate *Chlamydomonas* swims with opposing power strokes, yet synchronizes in phase in the familiar breaststroke. This indicates that a mechanism, internal to the cell, provides an additional flagellar coupling. Here we show that in comparison to the wildtype, markedly different synchronization states are found in *Chlamydomonas* mutants deficient in filamentary connections between basal bodies. Quantitative studies of complex flagellar coordination strategies found in quadri-, octo- and hexadecaflagellates reveal further evidence that intracellular couplings between flagellar basal bodies compete with hydrodynamic interactions to determine the precise form of flagellar synchronization in unicellular algae.

Keywords: *Chlorophyte — Prasinophyte — eukaryotic algae — internal coupling — flagellar synchronization — basal fibers*

## I. SIGNIFICANCE STATEMENT

*In areas as diverse as developmental biology, physiology and biomimetics there is great interest in understanding the mechanisms by which active hair-like cellular appendages known as flagella or cilia are brought into coordinated motion. The prevailing theoretical hypothesis over many years is that fluid flows driven by beating flagella provide the coupling that leads to synchronization, but this is surprisingly inconsistent with certain experimentally observed phenomena. Here we demonstrate the insufficiency of hydrodynamic coupling in an evolutionarily significant range of unicellular algal species bearing multiple flagella, and suggest the key additional ingredient for precise coordination of flagellar beating is provided by contractile fibers of the basal apparatus.*

## II. INTRODUCTION

Possession of multiple cilia and flagella bestows significant evolutionary advantage upon living organisms only if these organelles can achieve coordination. This may be for purposes of swimming [1, 2], feeding [3], or fluid transport [4, 5]. Multiciliation may have evolved first in single-celled microorganisms due to the propensity for hydrodynamic interactions to couple their motions, but was retained in higher organisms, to be found in such places as the murine brain [6] or human airway epithelia [7]. Since Sir James Gray first noted that “automatic units” of flagella beat in “an orderly sequence” when placed side by side [8], others have observed the tendency for nearby sperm cells to undulate in unison or aggregate [9, 10], and subsequently the possible hydrodynamic origins of this phenomenon have been the subject of extensive theoretical analyses [2, 5, 11]. Despite this, the exclusiveness and universality of hydrodynamic effects in the coordination of neighboring cilia and flagella remains unclear.

We begin by considering one context in which hydrodynamic interactions are sufficient for synchrony [12]. The alga *Volvox carteri* (VC) is perhaps the smallest colonial organism for which cellular division of labor is observed [13]. Adult spheroids possess two cell types: large germ cells interior of an extracellular matrix grow to form new colonies, while smaller somatic cells form a dense surface covering of flagella protruding from the matrix into the medium, enabling swimming. These flagella generate waves of propulsion which despite lack of centralized or neuronal control (“coxless”) are coherent over the span of the organism [14]. In addition, somatic cells isolated from their embedding colonies (Fig. 1A) beat their flagella in synchrony when held side by side sufficiently close to each other [12]. Pairwise configurations of these flagella tend to synchronize in phase when oriented with power strokes in the same direction, but antiphase when oriented in opposite directions, as predicted [15] if their mutual interaction were hydrodynamic in nature. Yet, not all flagellar coordination observed in unicellular organisms can be explained so simply. The lineage to which *Volvox* belongs includes the common ancestor of the alga *Chlamydomonas reinhardtii* (CR) (Fig. 1B), which swims with a familiar in-phase breaststroke with twin flagella that are developmentally positioned to beat in *opposite* directions (compare Fig. 1D with 1C). Yet, a *Chlamydomonas* mutant with dysfunctional phototaxis switches stochastically the actuation of its flagella between in-phase and antiphase modes [15, 16]. These observations led to the conjecture [15] that a mechanism, internal to the cell, must function to overcome hydrodynamic effects.

Pairs of interacting flagella evoke no image more potent than Huygens’ pendulum clocks [17]: two oscillating pendula will tend towards synchrony (or anti-synchrony) when attached to a common support, whose flexibility provides the necessary coupling. Here we present a diverse body of evidence for the existence of a biophysical equivalent to this mechanical coupling. In examining the ultrastructure of *Chlamydomonas* and related algae we find a likely candidate in the prominent fibers connecting pairs of basal bodies [18], which are known to have contractile properties. Such filamentary connections are completely absent in configurations of two pipette-held uniflagellate cells (Fig. 1A), and defective in a class of CR mutants known as *vfl* (Fig. 1B). We show in both cases that the synchronization states are markedly different from the wildtype breaststroke.

Seeking evidence for the generality of putative internal control of flagellar coupling in unicellular organisms, we use light microscopy, high-speed imaging and image-processing to elucidate the remarkable coordination strategies adopted by quadri-, octo-, and hexadecaflagellates, which possess networks of basal linkages between flagella that increase in complexity with flagella number. The flagellar apparatus, comprising basal bodies, connecting fibers, microtubular rootlets and the transition regions of axonemes, is among the most biochemically and morphologically complex structures occurring in eukaryotic flagellates [19]. The significance of basal coupling relative to passive hydrodynamics is highlighted, especially in maintaining the relative synchrony between pairs of diametrically-opposite flagella. Our study attempts to reconcile multiflagellar swimming with the geometric configurations of these flagella and that of their differing basal architecture. In the algal kingdom, the structure and assembly of basal bodies is intimately related to species phylogeny.

While key structural features of eukaryotic axonemes are conserved from algal to mammalian cilia/flagella (in terms of composition by microtubules, motive force generation by dyneins, or signal transduction by the radial-spoke/central pair [16]), far greater diversity exists in the strategies devised for flagellar coordination. Such strategies are especially important not only in unicellular microswimmers bearing relatively few flagella, but also in ciliary arrays. In mice defects in structures known as basal feet can cause ciliopathies [20], while the striated (kinetodesmal) fibers in *Tetrahymena* help maintain BB orientation and resist hydrodynamic stresses [21]. Insights from primitive flagellates may thus have broader implications.

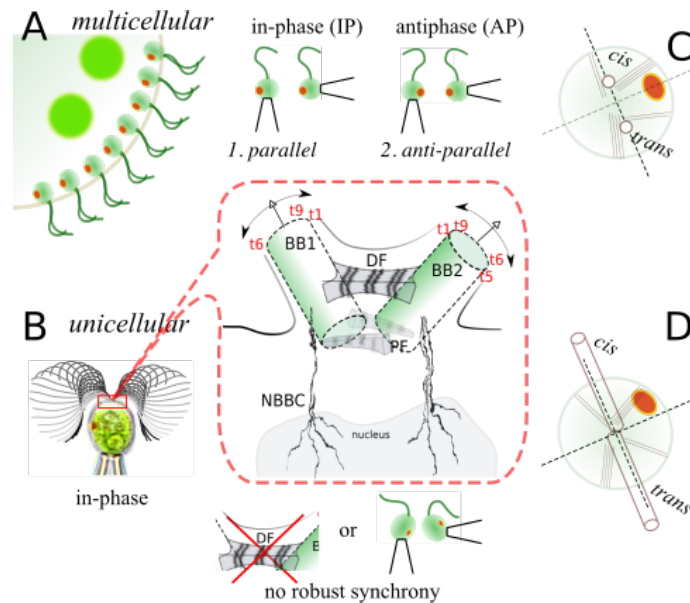


FIG. 1. Flagellar synchronization in multicellular vs unicellular algae. A) Somatic flagella isolated from *V. carteri* tend to synchronize either in IP or AP depending on relative orientation [12]. B) Despite maintaining its flagella in position 2, *C. reinhardtii* swims an in-phase breaststroke. This synchrony is altered i) upon mutation of basal fibers or ii) manipulation of two closely-separated uni-flagellate cells. [BB- basal body, DF - distal fiber, PF - proximal fiber(s), NBBC - nuclear-basal-body connectors. Arrows: plane of flagella beating. Numbered: triplet microtubules.] C)+D) Typical orientation of BBs, flagella, and positioning of microtubule rootlets in VC and CR.

### III. PAIRWISE INTERACTIONS BETWEEN FLAGELLA

The biflagellate condition may have undergone convergent evolution to appear in multiple lineages, in the naked green alga *Spermatozopsis similis* [22], in gametes of the seaweed *Ulva* [23], and in swarm cells of *Myxomycetes* [24]. The isokont case is exemplified by CR, and is best studied. Each ovoid cell ( $\sim 5 \mu\text{m}$  in radius) has two flagella  $1 - 1.5 \times$  body-length and distinguishable by BB age. During cell division each daughter retains one BB from the mother [25] which becomes associated with the *trans*-flagellum, while a second is assembled localizing near the eyespot and associates with the *cis*-flagellum (Fig. 1). When both flagella prescribe identical beat patterns a nearly planar breaststroke is achieved, which is highly recurrent and stable to small perturbations [26]. By modulating this bilateral symmetry cells accomplish reorientation. During phototaxis towards or away from light [27] photons incident on the eyespot activate voltage-gated calcium channels which alter levels of intracellular calcium, leading to differential bilateral flagellar responses.

Just as ionic fluctuations (e.g. calcium) can alter the beating of each flagellum, the synchrony of a pair is likewise mutable. Transient gait changes involving loss of synchrony and altered beating in one flagellum are manifest as ‘slips’ [16, 28], occurring stochastically at rates sensitive to such environmental factors [15, 26, 29] as temperature, light, chemicals, hydrodynamics, and age of culture. Altered beat during slips is analogous to the antiphase gait (AP) recently characterized in the phototaxis mutant *ptx1*, which displays stochastic transitions between a wildtype-like in-phase (IP) and the AP gait [15, 16]. In CR this dependence of biflagellar synchrony on physiology signifies the possibility for internal control by the cell above and beyond hydrodynamics [12], thereby motivating the present investigation.

*Variable flagella mutants.* Early work [18] identified fibers connecting the two *Chlamydomonas* BBs, including a  $300 \text{ nm} \times 250 \text{ nm} \times 75 \text{ nm}$  bilaterally symmetric distal fiber (DF), which bears complex striation patterns with a periodicity of  $\sim 80 \text{ nm}$  (Fig. 1b). Striation periodicity varies across species and in response to chemical stimuli, suggestive of an active contractile role [30]. The DF contains centrin, which likely contracts in response to calcium signals [31]. Centrin is also found in nucleus-BB connectors (NBBC) which are involved in localization of BBs during cell division [31]. The two BBs have an identical structure of 9 triplet microtubules which form a cartwheel arrangement [32]. Importantly, the DF lies in the plane of flagellar beating, and furthermore attaches to each BB at the *same* site relative to the beating direction of the corresponding flagellum (Fig. 1B). This inherent rotational symmetry makes the DF uniquely suited to coordinating the in-phase *Chlamydomonas* breaststroke.

Hypothesizing a key role for the DF in *Chlamydomonas* flagellar synchrony we assess the motility of the mutant *vfl3* (CC1686, *Chlamydomonas* Center), which is associated with DFs that are missing, misaligned or incomplete in a large percentage of cells [30]. Swimming is impaired, with many cells rotating in place near the bottom of the chamber. In this mutant the number of flagella (0 – 5), their orientation and localization on the cell body, as well as cell size are abnormal. While BBs occur in pairs, not every BB will nucleate a flagellum [33], thus allowing flagella number to be odd. However no structural or behavioral flagellar

defects were observed [30].

The six scenarios presented in Fig. 2A-F are representative of configurations of flagella found in *vfl3*, for cells bearing 2 or 3 flagella. Pairwise interactions between neighboring flagella are considered in the following. For each flagellum a phase  $\phi(t)$  was extracted from the high-speed imaging data by interpolating peaks in the standard deviation of pixel intensities measured across pre-defined regions of interest. We find that *vfl* flagellar beating frequencies are more variable than that of the wildtype, and as such we elect to determine phase synchrony between pairs of flagella via a stroboscopic approach. Given a pair with phases  $\phi_1, \phi_2$  we characterize the distribution  $\mathcal{P}_C(\chi)$  of

$$\chi = \phi_2 \bmod 2\pi \big|_{t:\phi_1 \bmod 2\pi = C}. \quad (1)$$

That is, the phase of flagellum 2 is measured *conditional* on the phase of flagellum 1 attaining the value  $C$ . From long timeseries we determine  $\chi$  by binning  $[0, 2\pi]$  into 25 equi-phase intervals centered around  $\{C_k, k = 1, \dots, 25\}$  to obtain the  $N_k$  corresponding time points for which  $\phi_1 \bmod 2\pi$  falls into the  $k$ th interval. The distribution of this conditional phase  $\chi^k := \{\phi_2(t_i), i = 1, \dots, N_k\}$ , which is peaked when the oscillators phase-lock and uniform when unsynchronized, can be displayed on a circular plot by conversion to a colormap. The results for  $k = 1$  are displayed in Fig. 2. The phase vectors can be summed and averaged to define a synchronization index

$$S = \frac{1}{25} \sum_k \left| \frac{1}{N_k} \sum_j \exp(i\chi_j^k) \right|, \quad (2)$$

so that  $S_k = 1$  (perfect synchrony) and  $S_k = 0$  (no synchronization).

Wildtype *Chlamydomonas* flagella operate over a large frequency range with little modification to the waveform; the intrinsic frequencies of *cis* and *trans* flagella may differ systematically by up to 30% under conditions of physiological stress, such as during deflagellation [16]. In the *vfl3* mutant, pairs of flagella with very different intrinsic frequencies cannot achieve 1 : 1 synchronization, but transient phase-locking is nonetheless observed. Configurations involving significant steric effects between nearby flagella (Fig. 2A) also reduce beat frequencies compared to the wildtype. Of particular interest are Figs. 2D&E, where a given flagella pair (within each group of 3) is strongly frequency coupled, and when oriented with power strokes parallel or anti-parallel (Fig. 1A) tend toward IP or respectively AP synchrony, consistent with hydrodynamic coupling [15, 34] (see SI Video 1).

We have demonstrated that without functional or complete DFs, biflagellate *vfl3* cells do not perform synchronous breast-strokes. While putative elastic constriction of the basal fibers has not yet been observed *in vivo* in wildtype cells, isolated and reactivated flagella apparatuses do form more acute opening angles when subjected to elevated extracellular calcium [35]. To isolate the hydrodynamic contribution to the pairwise interactions between beating flagella, an alternative to the removal of physical connectors by mutation is to use flagella belonging to *different* cells. As discussed below, these flagella then cannot be coupled other than through the immersing fluid.

*Two nearby Chlamydomonas cells.* In the first of these configurations, we removed one flagellum from each of two wildtype cells by mechanical shearing (Fig. 3A). Recognizing that *cis* and *trans* flagella are functionally distinct [16, 36], the aim is to assemble a *Chlamydomonas*-like arrangement comprising a *cis* and a *trans* flagellum from two *different* cells (Materials and Methods). Despite similarity with the wildtype configuration, no sustained IP breaststrokes were obtained; instead, closely separated ( $<5 \mu\text{m}$ ) pairs tend to AP synchronization. Beat frequencies of these isolated *cis* or *trans* flagella are more noisy than the wildtype and consequently measured phase-locking is not robust ( $S = 0.08$ ). The conditional (stroboscopic) phase  $\chi$  (Fig. 3A) is peaked weakly about  $\pi$ , but the two flagella can also show IP synchronization, albeit transiently. The IP gait becomes preferred when the flagella nearly touch at certain phases of their beat cycles, and are then driven by fluid-structure interactions into parallel conformation [37]. Such stochastic transitions between IP and AP states are reminiscent of flagellar dynamics in the mutant *ptx1*, which also exhibit stable IP and AP gaits [15]. We shall return (see Discussion) to the implications of the above for the mutation giving rise to the unusual flagellar synchronization in *ptx1*.

The similarity over time of the two waveforms in any given state (IP or AP) can be compared. For ease of visualization, waveforms discretized at equidistant points are ordered from base to tip:  $\mathbf{f}_i^L, \mathbf{f}_i^R$  for  $i = 1, \dots, N_p$ . These are transformed by rotation with matrix  $\mathcal{T}$  about a reference axis connecting the basal bodies according to  $\mathbf{f}^L \rightarrow \mathbf{f}'^L = \mathcal{T}(\mathbf{f}^L - \mathbf{m})$  and  $\mathbf{f}^R \rightarrow \mathbf{f}'^R = \mathcal{T}(\mathbf{f}^R - \mathbf{m})$ , with  $\mathbf{m} = (\mathbf{f}_1^L + \mathbf{f}_1^R)/2$ , and then translated to the origin (Fig. 3A).

The synchronization index in Eq. 2, while suitable for distinguishing phase-locked and unsynchronized states, does not discriminate between AP and IP states. Instead, the perpendicular deviation

$$d(t_i, s_j) = [(\mathbf{f}^L(t_i, s_j) + \mathbf{f}^R(t_i, s_j))/2 - \mathbf{F}(t_i, s_j)] \cdot \mathbf{n} \quad (3)$$

of the pairwise average waveform from the linear base-to-tip direction  $\mathbf{F}$  is correlated with the state of phase synchronization (Fig. 3A), where  $t_i$  is the frame index,  $s_j$  indexes the arclength discretization, and  $\mathbf{n}$  is a unit vector satisfying  $\mathbf{n} \cdot \mathbf{F} = 0$ . For

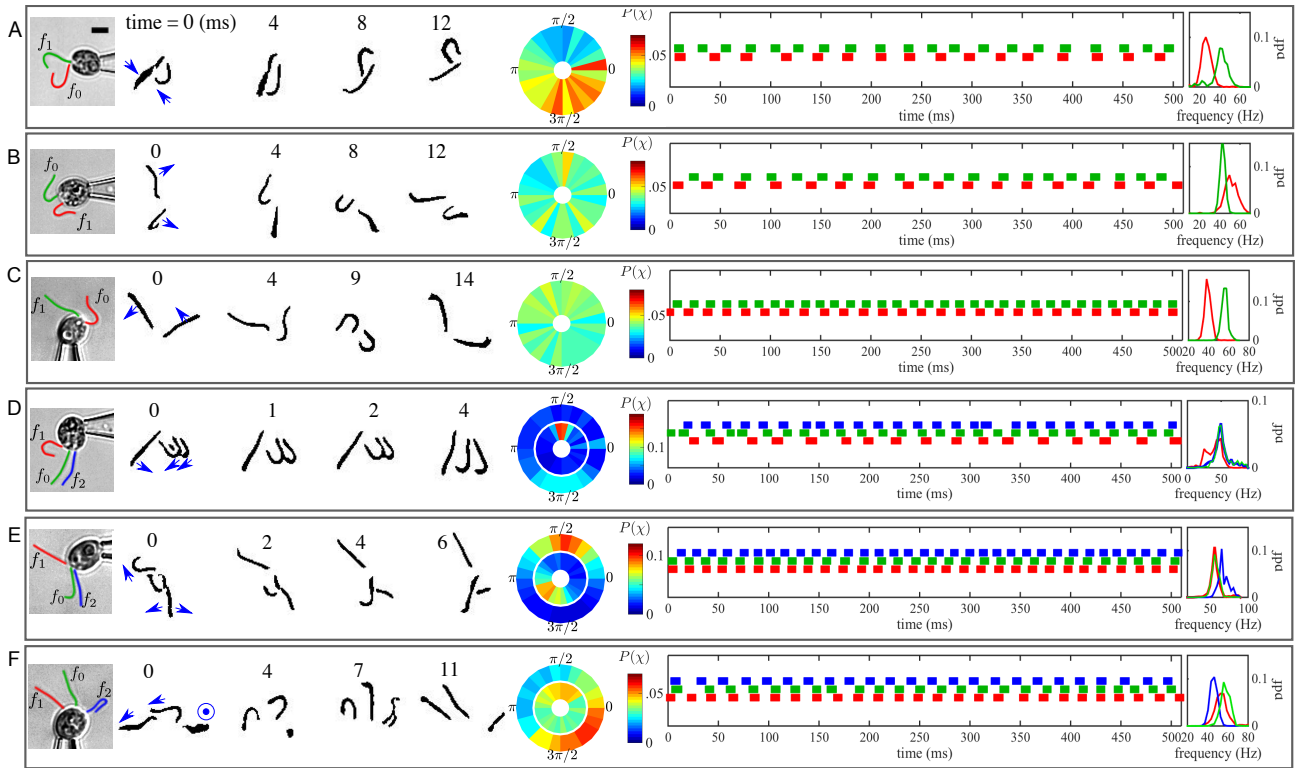


FIG. 2. The *Chlamydomonas* mutant *vfl3* is defective in the distal striated fibers, and present abnormal flagella number as well as orientation. Scale bar:  $5 \mu\text{m}$ . Synchronization is investigated for configurations of 2 flagella in (A,B) toward-facing or away-facing flagella-like (FL) orientations, or (C) cilia-like (CL) orientation, and of 3 flagella: including a CL-oriented pair (D) or FL-oriented pair (E), and case (F) where one flagellum is pointing out of the page. Arrows indicate the power stroke direction of each flagellum. In each case distributions of phases  $P_0(\chi)$  of flagella  $f_{1,(2)}$  conditional on the phase of flagellum  $f_0$  are shown on circular plots (in D-F:  $f_1$  for the inner ring and  $f_2$  for the outer), to give  $S_{1,0} = 0.20, 0.04, 0.04$  for A-C, and  $(S_{1,0}, S_{2,0}) = (0.30, 0.49), (0.53, 0.40), (0.02, 0.01)$  for D-F respectively. Phases are also discretized as "footprints" with length proportional to the duration of the current beat cycle, and plotted with corresponding pdfs of beat frequencies.

both IP and AP phase-locking states  $d$  defines a pattern resembling a travelling wave with frequency equal to the phase-locked frequency, propagating from flagellum base to tip. The total deviation

$$d(t_i) = \sum_{j=1}^{N_p} d(t_i, s_j) \quad (4)$$

oscillates with larger amplitude during AP than IP (Fig. 3).

*Two nearby V. carteri somatic cells.* In the second scenario (Fig. 3B), pairs of pipette-held *Volvox* somatic cells (normally biflagellate) were similarly rendered unflagellate [see also [12]]. Shape functions of transformed flagellar waveforms indicate a preference for AP synchronization, though the IP is also observed (see SI Videos 2 & 3). Accordingly, the phase stroboscope is strongly peaked near  $\chi = \pi$  ( $S = 0.67$ ). The existence, stability, and frequency of IP and AP states are wholly consistent (see SI Text), with a basic theory [34] in which a pair of hydrodynamically coupled flagella can be modelled as a pair of beads rotating on springs with compliant radii  $R$  separated by a distance  $\ell$ . Assuming  $R \ll \ell$ , this model predicts that either IP or AP states of synchrony are most stable depending on whether the beads are co- or counter-rotating [15, 34]. The validity of these assumptions must be reevaluated when proximity between flagella leads to non-local hydrodynamic interactions between different portions of the flagella, and consequently interactions between the undulating filaments become highly sensitive to their initial relative phase difference [37]. Note how the beats of *Volvox* somatic flagella differ from that of *Chlamydomonas* by a distinctive upward tilt of the beat envelope, which is consistent with a modification of BB orientation (Figs. 1C&D) (presumably to facilitate its function within the geometric confinement of the embedding colony).

In this section, we have established that hydrodynamic synchronization alone cannot explain the in-phase coordination of the *Chlamydomonas* breaststroke. More generally we find algal flagella to be deformable by hydrodynamic loading. It is precisely because of this propensity for flagella beating to be deformed by flow disturbances such as those generated by the motion of nearby flagella, that an internal control mechanism must be present to compensate in such cases where interactions through

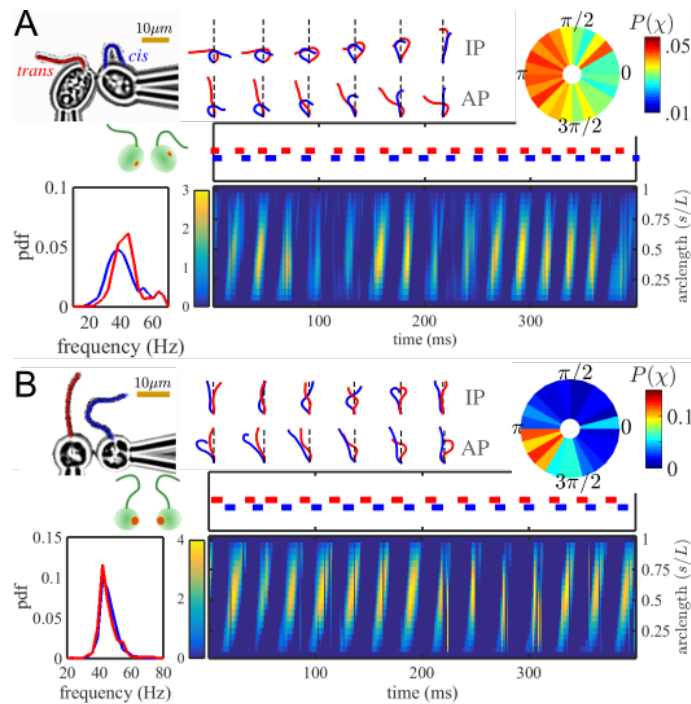


FIG. 3. Coupling of flagella by hydrodynamics. Pairwise interactions between A) two CR flagella (one *cis*, one *trans*) and B) two uni-flagellated VC somatic cells. Frequency locking (here) leads to IP or AP states with a preference for AP, but phase synchronization is more robust in B than in A. For each pair, the deviation  $d$  computed from the pairwise shape average  $\bar{f}$  (see text) evolves periodically and propagates as a travelling wave.

the fluid are contrary to the desired mode of propulsion by flagella. Next, we investigate unicellular algae with more than two flagella and hence increased complexity of flagellar coordination, in search of evidence in support of this hypothesis.

#### IV. MULTIFLAGELLATION

It has long been proposed that Volvocine green algae derived from *Chlamydomonas*-like ancestors. Since then, the classification of Viridiplanta (green plants) has undergone repeated revisions due to the enormous variability that exists in the form and structure exhibited by its member species. For collections of flagella-bearing green algae, developmental features including mitosis and cytokinesis as well as morphological features including the number, structure, or arrangement of flagella, and even the nature of body coverings such as scales and theca, have served as key diagnostic tools for mapping the likely phylogenetic relationships between species [38, 39].

*The flagellar apparatus.* The two CR BBs, which emerge in a V-shape from the anterior pole at  $70\text{--}90^\circ$  (Fig. 1B), arrange with near radial symmetry and a clockwise (CW) offset characteristic of advanced biflagellate algae. However many evolutionarily more primitive flagellates have BBs oriented with a counter-clockwise (CCW) offset [40]. For each species, only one absolute configuration of BBs exists and its mirror-symmetric form is not possible [41]. Linkages or roots connecting BBs, either microtubular or fibrillar, are key systematic characters. For each BB, two microtubular roots (termed left and right when viewed from the distal end) emerge from and attach to specific triplets in the transition region. These roots were probably asymmetric in very early flagellates [40], which subsequently doubled with the second set rotated  $180^\circ$  from the first. The right root is generally 2-stranded; denoting the strand-number of the left root by  $X$ , together these form the X-2-X-2 cruciate system characteristic of advanced green algae [ $X = 4$  in CR [18]]. Fibrillar roots, classified [39] as system I (associated with microtubules) or II (including rhizoplasts which have contractile properties), occur in yet larger numbers in algae with increasing flagella number. Each BB is unique up to the imbrication of its member tubules, and a constant positional relationship pertains between its two roots and a principal connecting fiber that links the two ontogenetically oldest BBs (1 and 2). It is this connecting fiber that is mutated in the *vfl* mutants (Fig. 2). Precise lineage-tracing has led to a consistent numbering system for BBs which greatly facilitated the study of flagellar transformation in algae with  $> 2$  flagella, which we adopt [41, 42].

*Quadri-flagellate.* We selected a number of species of evolutionary interest and discovered novel strategies for coordinating four flagella (Fig. 4 and SI Video 4). Quadri-flagellate swimming gaits are found to involve particular phase relationships between flagella, which by analogy with quadruped locomotion, may be reproduced by coupled networks of nonlinear oscillators that

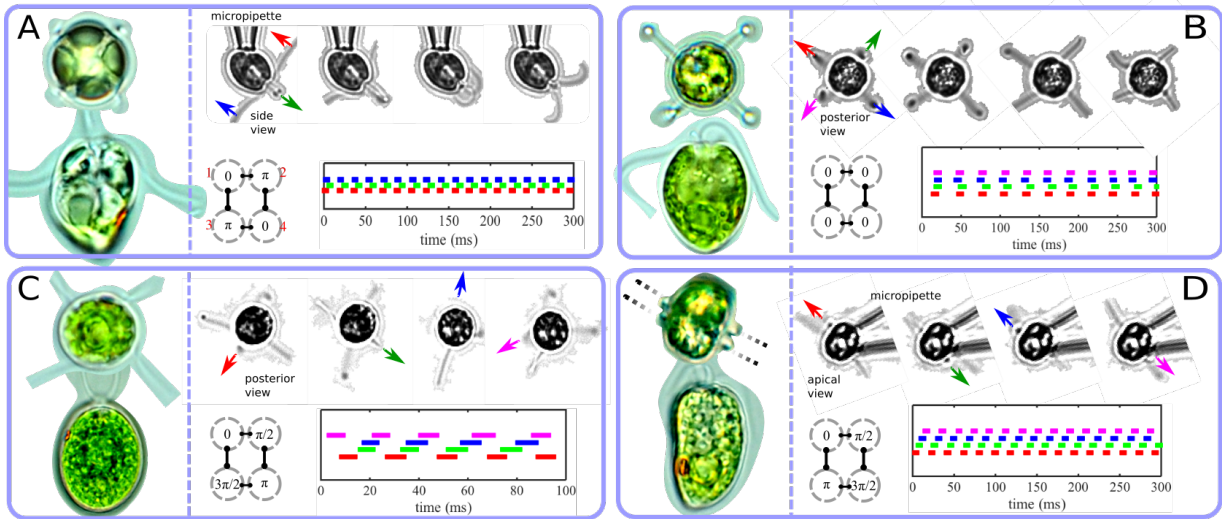


FIG. 4. Analogues to the gaits of a quadruped, quadriflagellate swimming involves diverse gaits of actuation of four flagella that is species specific: including the A) trot (*Pyramimonas parkeae*), B) pronk (*Pyramimonas tetrahynchus*), C) rotary gallop (*Carteria crucifera*), and D) transverse gallop (*Tetraselmis suecica*)

are controlled by a central pattern generator or equivalent [43, 44]. Any given spatial symmetry of four flagella corresponding to dynamical states  $\mathbf{X}_j$  (indexed by flagellum  $j = 1, 2, 3, 4$ ) is represented as a permutation  $\sigma$  of  $\{1, 2, 3, 4\}$ , so that  $\mathbf{X}_k(t) = \mathbf{X}_{\sigma(k)}(t)$  for all times  $t$ . Periodic gaits also possess temporal symmetries: if  $T$  is the gait period, then for each oscillator  $k$ ,  $\mathbf{X}_k(t) = \mathbf{X}_k(t + T)$  for all  $t$ . We normalize  $T$  to  $2\pi$  and consider invariance of flagella under phase shifts  $\phi$  taken modulo  $T/2\pi$ ; the pair  $[\sigma, \phi]$  denotes a spatial-temporal symmetry of the  $\{\mathbf{X}_j\}$ , where

$$\mathbf{X}_k(t) = \mathbf{X}_{\sigma(k)}(t - \phi). \quad (5)$$

and  $k = 1, \dots, 4$ . The symmetries of the underlying coupled oscillator network admits a symmetry group under the composition rule:

$$[\sigma_1; \phi_1] \circ [\sigma_2; \phi_2] = [\sigma_1\sigma_2; \phi_1 + \phi_2], \quad (6)$$

which can be matched to known quadruped or quadriflagellate gaits. In algae, the form of underlying coupling is constrained by the configuration of BBs and the arrangement of connecting fibers. A particularly extreme case occurs when two biflagellate CR gametes fuse during sexual reproduction [45] to form quadriflagellate dikaryons. In this transient stage, original DFs remain but no additional structures form between pairs of unlike mating type; strong hydrodynamic coupling due to their physical proximity leads to a striking *double* bilateral breaststroke (SI Video 5).

In a simple scenario we consider a rectangular network and allow for pairwise coupling to be one of two types (Fig. 4). In cycle notation (where  $(ij)$  means interchange of  $i$  and  $j$ ), spatial symmetries include  $\iota$  (the identity, fixing everything),  $\sigma = (12)(34)$  (reflection in the  $y$  axis),  $\rho = (13)(24)$  (reflection in the  $x$  axis), and  $\sigma\rho = (14)(23)$  (interchange of both diagonals) [43]. Table 1 displays and names gaits which possess such symmetries; of these, only 4 and 5 are not observed in algae. Several quadriflagellates display the identity permutation corresponding to a rest phase during which all flagella are temporarily stationary [46], and different gaits occur in specific species (Fig. 4). To facilitate interpretation we consider for measured flagellar phases  $\psi_j$  the matrix  $\Delta_{ij} = \psi_i - \psi_j$  ( $i, j = 1 \dots 4$ ) of phase differences satisfying  $\Delta_{ij} = \Delta_{ji}$ ,  $\Delta_{ii} = 0$ , and  $\Delta_{ik} = \Delta_{ij} + \Delta_{jk}$ . Each gait is associated with a 3-tuple:  $[\Delta_{12} \Delta_{13} \Delta_{14}]$  (Fig. 4).

Distinct genera of quadriflagellates, including the marine Prasinophyte *Pyramimonas*, swim with two pairs of precisely alternating breaststrokes in a gait akin to the ‘trot’ (#3, Table 1; SI Video 4). The Prasinophytes are a polyphyletic class of green algae united through lack of similarity with either of the main clades: the Chlorophyta and Streptophyta. The four isokont flagella of *P. parkeae* (Materials and Methods) insert anteriorly into an apical pit or groove, emerging in a cruciate arrangement (Fig. 4A). The phase relation  $[\Delta_{12} \Delta_{13} \Delta_{14}] = [\pi \ 0 \ \pi]$  is seen in both free-swimming and micropipette-held cells. Interestingly, we find that the colorless Chlorophyte alga *Polytomella* (sp. *parva*), thought to have evolved by cell doubling along a direct line of descent from *Chlamydomonas* [47], also displays this gait.

Two further gaits (SI Video 4) are presented in the type *Pyramimonas* species *P. tetrahynchus* [48], a freshwater alga (Materials and Methods). The first, which we term the ‘pronk’ (#2, Table 1), has all four flagella synchronized with zero phase difference (Fig. 4C). The second possesses fewer symmetries: flagella beat in a sequence typical of the transverse gallop in

TABLE I. Quadriflagellate vs quadruped: gaits and their symmetries. Only those entries shown in red have not been observed in algae.

gait #	symmetries	context
1 (stand)	$[\iota; \phi], [\sigma; \phi], [\rho; \phi], [\sigma\rho; \phi]$	algae, quadrupeds
2 (pronk)	$[\iota; 0], [\sigma; 0], [\rho; 0], [\sigma\rho; 0]$	algae, gazelles
3 (trot)	$[\iota; 0], [\sigma; \pi], [\rho; \pi], [\sigma\rho; 0]$	algae, horses
4 (bound)	$[\iota; 0], [\sigma; \pi], [\rho; 0], [\sigma\rho; \pi]$	squirrels
5 (pace)	$[\iota; 0], [\sigma; 0], [\rho; \pi], [\sigma\rho; \pi]$	camels
6 (transverse gallop)	$[\iota; 0], [\rho; \pi]$	algae, horses
7 (rotary gallop)	$[\iota; 0], [\sigma\rho; \pi]$	algae, dogs

quadrupeds (#6, Table 1). *P. tetrahynchus* swims preferentially with the latter gait, while pronking is more likely to occur when the cell escapes from walls/obstacles, or when changing direction. The rotary gallop, in which flagella move CCW in sequence (# 7, Table. 1, SI Video 4) occurs in the Volvocale *Carteria crucifera* (a close relative of *Chlamydomonas*).

*Tetraselmis*, a Prasinophyte comprising both freshwater and marine species, also displays the transverse gallop (Fig. 4B). Cells, measuring 10 – 20  $\mu\text{m}$  in dimensions, have short, thick, scaly flagella which are covered in rows of hair-scales that align transversely to the power stroke directions of the attached flagella. We examine the motility of the marine alga *T. subcordiformis* (Stein), for which the precise basal architecture is known [49]. The four flagella emerge nearly parallel from an apical depression, separating distally into pairs according to the pairing and orientation of BBs, with power stroke directions shown (Fig. 4B). An alternate synchronous gait of four flagella has been reported in this species [50], but was not observed under our experimental conditions.

*Prevention of beating of one flagellum.* What single mechanism can give rise to such diversity of gaits? Symmetries of free-swimming, pipette-held or surface-bound gaits (Fig. 4) are species- rather than drag- dependent. Coordination by hydrodynamic interactions alone thus seems unlikely, as further evidenced by the following experiment. Given a quadriflagellate exhibiting a certain gait we wish to disturb the beat pattern of one flagellum to observe its effect on the synchrony of the remainder. Fig. 5A depicts a pipette-immobilized *Tetraselmis* cell with flagella free to beat in a pattern qualitatively similar to free-swimming cells observed under identical conditions. *Tetraselmis* is thecate, and thus for micromanipulation purposes is preferred over *Pyramimonas* which only have scale-coverings. The flagella maintain phase relations indicative of the transverse gallop discussed earlier Fig. 5B. Beating in one flagellum was then completely stalled using a second, narrower pipette. It is seen that the remaining three flagella continued as before, in keeping with the same relative phase dynamics (Fig. 5C). This remarkable ability to maintain the prior coordination pattern strongly implicated internal beat modulation, for instance by active contractility. Furthermore a freely swimming cell can rapidly reestablish the same coordination of its flagella during abrupt gait changes, such as after a shock event [46].

*Octoflagellate.* Within the Prasinophytes considerable variation exists in its > 16 genera and > 160 species, concerning not only the arrangement of flagella but also its number [51]. Of these only 3 species of *Pyramimonas* are known to have eight flagella during all or parts of its cell cycle [52–54], and only one has sixteen [55]. Cells of *P. octopus* measure  $\approx 20 \mu\text{m}$  in length, with yet longer flagella (twice) whose distal portions are folded and highly curved beside the cell. Cells swim at  $\sim 200 - 300 \mu\text{m/s}$  along helical trajectories. The rare state in which a cell's longitudinal axis is transverse to the imaging plane (Fig. 6B) can be prolonged by increasing the medium viscosity (Materials and Methods). Diametrically opposite groups (usually but not exclusively pairs) of flagella beat synchronously with phase shifts between neighbouring pairs (Fig. 6A, SI Video 6). In-phase coupling is more robust in some pairs than in others, which may be directly related to the intrinsic BB architecture (see Discussion and Fig. 8). The orientation of swimming strokes is consistent with observed sense of cell-body rotation, CW when viewed from above.

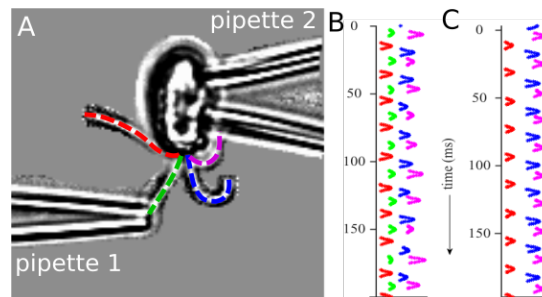


FIG. 5. Preventing the beating in a flagellum of *T. suecica* using a second micropipette results in little change in the relative coordination in the remainder. Sequences of flagellar "footprints" (labelled by color according to A) are measured before (B) and after (C) manual stalling of one flagellum.



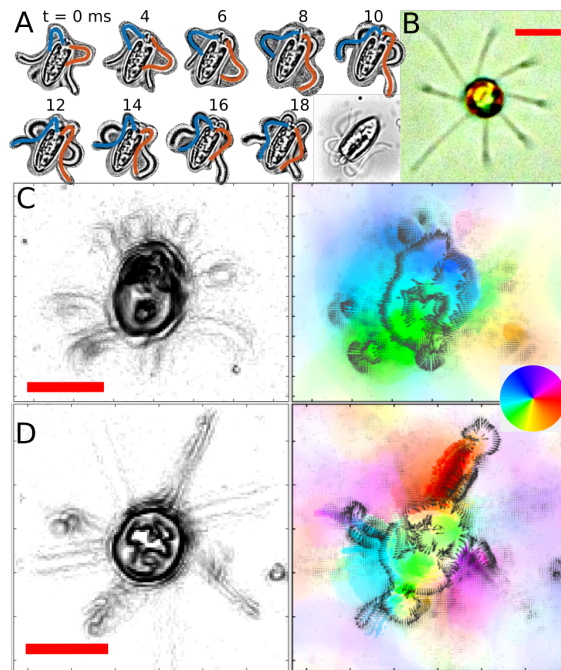


FIG. 6. Free-swimming *P. octopus*. A) A cell performing pairs of IP breaststrokes in sequence: waveforms of one pair are highlighted, B) one in a static stand gait in which no flagellum is active. C-D) Gradient images (left) identifying the active flagella, optical flow field (right) showing direction and magnitude of the estimated flow disturbance. All flagella are active in C but only the next-nearest neighbor flagella in D. Scale bars:  $10\ \mu\text{m}$ .

Free-living *P. octopus* cells also exhibit settling behavior in which *all* flagella cease to beat (Fig. 6B); this octoflagellate “stand” gait is compatible with its benthic nature. Resumption of beating usually involves simultaneous activation of all 8 flagella (pronking), but within only 2 or 3 beats the exquisite pairwise coordination associated with normal swimming is reestablished [46]. Gait changes in cells responding to noise or physical interaction with obstacles (mechanosensation) involve more unusual combinations. We summed successive gradient images to identify actively beating flagella: all 8 in Fig. 6C (left) but only 4 of 8 in Fig. 6D (left). These extent of these actuation patterns can be seen by visualizing the flow disturbance imparted by the flagellar beating using an optical flow technique to monitor the migration of image pixels between frames, visualizing the flow direction and magnitude by color and color intensity [56] (see also Computer Vision toolbox, MATLAB, The MathWorks Inc.). Contrary to conventional PIV-based methods, here there is no need to seed the solution with foreign particles or tracers, and flow directions and even flow magnitudes of salient objects can be obtained directly from the optical data. Components of the 2D flow field were determined by minimizing an objective function subject to certain global (smoothness) or local (fidelity) constraints (Fig. 6); pixels belonging to the same object are likely to retain their prior intensity values at later times. We observe (Figs. 6C&D, right) that flow maxima occur near the apex where the flagella emerge, decaying rapidly away from the cell body.

*Hexadecaflagellate*. Only one species is known to possess 16 flagella: with cells measuring up to  $40\ \mu\text{m}$  in length, the arctic species *P. cyrtoptera* is the largest *Pyramimonas* recorded, and its 16 flagella (32 when dividing) which are longer than the cell and emerge radially from a deep anterior flagellar pit (Figs. 7A&B), is the highest number ever reported in a phytoflagellate [55]. This species is also benthic and uses its flagella to attach to icy surfaces. It is closely related to *P. octopus* [57], and is thought to have evolved when an octoflagellate failed to divide after duplication of chloroplasts and flagella. The species name *P. cyrtoptera* originates from the Greek for *cyrto* meaning “curved” and *pteron* meaning “wing”, referencing the cell morphology (Fig. 7). Light microscopy reveals a lobed structure with two pairs of split eyespots and the presence of two chloroplasts (Fig. 7C). *P. cyrtoptera* cells are stenothermal and euryhaline: growth becomes limited above  $7\text{-}8^\circ\text{C}$ . Once removed from their natural habitat where temperature variations are typically  $< 2^\circ\text{C}$ , cell cultures have proved fragile and difficult to maintain in laboratory conditions.

Hexadecaflagellate swimming presents an intriguing circumstance in which the distance of separation between flagella is so small that hydrodynamic coupling is inevitable. When fully splayed (Fig. 7B) the 16 flagella are separated on average by  $360/16 = 22.5^\circ$  or  $7.85\ \mu\text{m}$  measured at a radial distance of  $20\ \mu\text{m}$  from the cell, compared to  $360/8 = 45^\circ$  and twice this distance in *P. octopus*. In *P. cyrtoptera* the interflagellar distance is thus far below the critical length for pairwise hydrodynamic synchronization [12]. A number of observed gaits involve hydrodynamically induced synchrony between some or even all flagella (SI Video 7). Rather than determine the positions of each individual flagellum, we use the envelope traced by the simultaneous propagation of flagella as proxy for the phase during the beat cycle, to obtain a frequency of  $\sim 25\ \text{Hz}$  for its

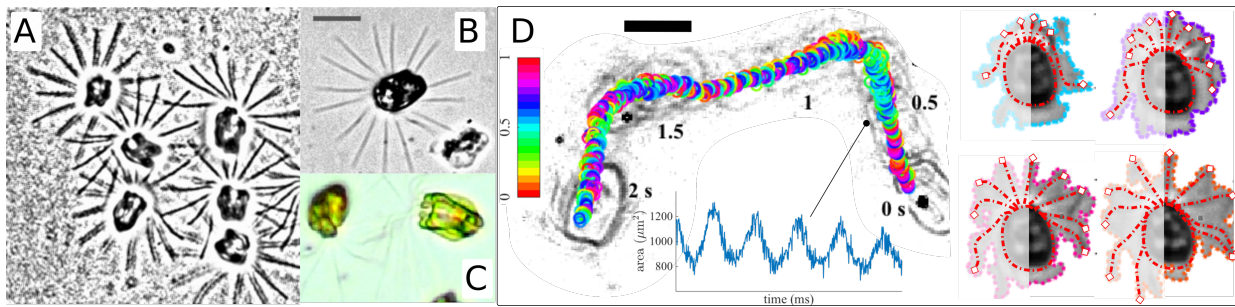


FIG. 7. The rare Arctic species *P. cyrptoptera* is the largest *Pyramimonas* known. All 16 flagella can spontaneously cease to beat and the cell can remain in this rest state for seconds (A-B). Cells,  $\approx 40 \mu\text{m}$ , are yellow-green and lobed (C). Pronking (D) is a common gait in this flagellate (SI Video 7): its periodicity can be determined by converting the area bounded by the flagella (far right) into a phase (normalized to  $[0, 1]$ ). The trajectory of a free-swimming cell is colored by phase (colorbar) during  $\sim 2$  s of continuous tracking. Inset: time series of the flagellar envelope area over five cycles. Scale bars:  $20 \mu\text{m}$ .

periodic evolution during the pronking gait (Fig. 7D). Symplectic metachronal waves have even been observed in cells trapped near surfaces (SI Text).

## V. DISCUSSION

**Insufficiency of hydrodynamics.** We have characterized flagellar synchrony in select mutants and in species of flagellates exhibiting swimming gaits that are unsustainable by passive interactions through the fluid, showing that known hydrodynamic theory cannot explain all cooperative or synchronization phenomena occurring among cilia and flagella. Thus the physical principle responsible for coordinating collective ciliary beating in *Volvox* or *Paramecium* differs from that responsible for precise patterns of beat organization occurring in unicellular microswimmers bearing only relatively few flagella. In the former case hydrodynamic coupling between flagella is sufficient [12], but in the latter (especially for obligate autotrophs) there is far greater incentive for an efficient swimming strategy that is actively modulated and robust *in spite of* hydrodynamic perturbations. Our approach was motivated in part by the freestyle gait (AP) in the CR phototaxis mutant *ptx1*, realizing that the wildtype IP breaststroke cannot be readily reconciled with hydrodynamic theory [15, 16]. A role for cell-body rocking in free-swimming cells has been proposed as an alternative to explain biflagellar synchrony in free-swimming wildtype CR [58], but this does not fully account for the motility of isolated and reactivated flagellar apparatuses [35], or for the dependence of synchronization on such extracellular factors as temperature or ionic composition of the medium [26]. In fact, pairs of *Chlamydomonas* flagella can be entrained by periodic hydrodynamic forcing, but the strength required greatly exceeds physiological values [59].

An additional ingredient, internal to the cell, is thus necessary to maintain IP biflagellate synchrony in CR and related species. Lack of pairwise synchrony in *vfl3* mutants defective in the DF (Fig. 2) strongly implicates said structure in this function. Indeed, BBs fulfil dual roles of nucleating/anchoring flagella as well as centrioles during cell division (in CR ensuring assembly of one *cis* and one *trans* flagellum per cell). In contrast, *ptx1* is thought to possess two *trans*-like flagella [60]. Mutations pertaining to the basal apparatus can simultaneously affect DFs and also BB duplication and segregation [30]. If fibrous BB connections are disrupted or weakened in *ptx1*, the resulting reduction in internal coupling or control of the flagella pair would then explain the stochastic reversion to an AP mode which is more in line with hydrodynamic predictions [15]. Future work should seek to examine flagellar apparatuses of *ptx1* under electron microscopy.

**Intracellular coordination by contractility.** The insufficiency of hydrodynamics suggests internal control by elastic, chemical, or mechanical means. This is supported by Figure 5, in which immobilization of one flagellum in a quadriflagellate has little effect on the coordination of the remaining three. More generally in free-swimming multiflagellates, spontaneous cessation of beating can occur in one or more flagella, leading to a variety of gait bifurcations. The BB from which each flagellum nucleates is a center for conduction of morphogenetic and sensory information between flagella and other intracellular organelles. Although BBs are not essential for flagellar function (isolated axonemes continue to beat when reactivated in ATP [61, 62]), they may contribute to coordination via inter-BB connections that in many species are contractile [63]. In CR robust NBBCs descending near the DF link BBs to the nucleus (Fig. 1B) remain intact even after detergent lysis treatment [31], and can be induced by calcium to undergo significant contraction [64]. Scaly algae including *Pyramimonas* and *Tetraselmis* possess an analogous structure termed a rhizoplast (Fig. 8) which can contract and relax cyclically [39, 50]. Such structures under tension experience much distortion during *active* beating, as observed from misalignment of fiber striation patterns [65]. Contraction occurs during live beating and is ATP-dependent in *Polytomella* [66], in real-time in paralyzed flagella and temperature sensitive mutants of *Chlamydomonas* [67], and to an extraordinary degree in *Microthamnion* zoospores [68]. ATPase activity has also been identified in the rod cells of the human eye where a large striated root attaches to the BB of a short (non-motile) cilium

[69].

**Ultrastructure and geometry of the flagellar apparatus.** Across algal species the totality of different gaits is numerous and varied (Figs. 4,6&7), implicating existence of a controller or pattern generator, whereupon transduction of putative ‘neural’ or pacemaker signals would then be mediated by the complex basal architecture. Flagellar apparatuses imaged by electron microscopy reveal networks of internal connections that are species-specific, and moreover increasing in complexity with flagella number [19]. Symmetries of this underlying network of structural couplings [43] likely translate downstream into symmetries of observed multiflagellate gaits (Fig. 8).

In *P. parkeae*, which consistently swims with two alternating pairs of IP breaststrokes (Fig. 4A), a (striated) prominent distal fiber (synistosome) links the central BBs 1, 2, and attaches to specific BB triplets [70]. Likewise a similar gait is observed by *Polytomella parva*, whose basal apparatus also displays diagonal symmetry (the flagella form opposing V-shaped pairs [71]). On the other hand, in *C. crucifera* BBs insert into an anterior papilla at the corners of a square (a cruciate pattern termed class II *sensu* Lembi [72]) and are tilted unidirectionally in contrast to the conventional V-shape found in *Chlamydomonas* and *Polytomella*. Distal fibers, rather than link directly to BBs, attach instead to electron-dense rods extending between them [72]. This unusual rotational symmetry is consistent with the prominence of the rotary gait in this species (Fig. 4B). In *Tetraselmis*, the flagella configuration is different still, separating distally into two nearly collinear pairs (Fig. 4D) with BBs forming a single zig-zag array (Fig. 8), in a state thought to have arisen from rotation of two of the flagellar roots in an ancestral quadriflagellate. Transfibers (closely-related to the *Chlamydomonad* PF and DF) connect alternate BBs, while BBs within the same pair are linked by Z-shaped struts [49]. Large rhizoplasts extend proximally toward the nucleus, forming specific connections with disc complexes and BB triplets. During free-swimming cells display frequent directional changes that are likely mediated by the extraordinary contractility of the rhizoplasts [50].

In the octoflagellate *P. octopus* (Fig. 6) BBs arrange asymmetrically in a diamond configuration which is partially open to accommodate nuclear migration during mitosis, and reflects the semi-conservative nature of BB duplication [73]. In dividing *P. octopus* 8 new BBs form peripheral to the existing ones [42]. The innermost pair of BBs (1, 2) assume the new position 1 in the two daughter cells (i.e. full maturation) after round 1 of cell division, but BBs 3, 4 and 5-8 only reach maturation respectively after rounds 2, 3 [42, 54]. More generally, all  $2^n$  BBs in a given cell reaches and thereafter remains at position 1 by the  $n$ th generation (cf *P. cyrtoptera* [55]). As in many *Pyramimonas* species, BBs 1, 2 are connected by a large synistosome. In *P. octopus* up to 60 individual connecting fibers establish specific connections with certain BB triplets, in addition to 6-8 rhizoplasts linking the basal apparatus to the nucleus. An even greater number of rhizoplasts and connecting fibers of varying sizes exists in the basal apparatus of *P. cyrtoptera*, but their identities were never resolved fully because of the untimely death of T. Hori [74]. It is also possible to determine the orientation of flagellar power strokes from electron-micrograph sections through the basal apparatus, which in *P. octopus* reveal a sequential CCW rotation [42, 54] consistent with sense of cell body rotation (SI Video 5). As in other scaly flagellates such as *Tetraselmis* and *Scherfferia*, the flagellar beat plane, as defined by triplets 1, 5-6, is further delineated by longitudinal rows of hair scales (“Melkonian’s rows”) [42]. The particular attachment of contractile fibers to the “weaker” side (BB triplets 6-9) suggest they may function to pull the flagellum back from each power stroke, facilitating the extraordinary coordination of *P. octopus* flagella.

**Evolution of multiflagellation among Viridiplantae.** As a cellular appendage, cilia, flagella, and the 9 + 2 axoneme prevails across eukaryotes and particularly the green algae; yet beyond the universality of this basic machinery much variability persists in the placement of organelles and external structures, form of flagellar insertion, and consequently in the diversity of strategies devised for algal flagellar coordination (Fig. 8). The basal apparatus is that rare structure which is both universally distributed and stable enough to infer homology across large phylogenetic distances, and yet variable enough to distinguish between different lineages. Representative species of flagellates considered here express  $2^n$  flagella, with much conservatism in the bi- or quadri-flagellate condition. As exemplified by *P. octopus* and *P. cyrtoptera*, the sparsity of species bearing > 4 localized flagella may stem from the difficulty and energetic costs of devising a flagellar apparatus capable of maintaining the desired coordination strategy in the presence of hydrodynamic coupling.

Since an early flagellate ancestor phagocytosed a prokaryote (eventually the chloroplast) >1 billion years ago, green algae have acquired capabilities for photosynthesis and autotrophism [75]. Their radiation and division into the clades of Streptophyta and Chlorophyta [76] has been corroborated by modern high-throughput chloroplast genome sequencing [77]. Occupying a basal phylogenetic position are *Prasinophytes* comprising primitive and morphologically diverse species including *Pyramimonas* [40]. These algae have conspicuous body and flagella scales which are precursors of theca and *Volvoclean* cell walls [41]. Importantly, it is the quadriflagellate conditions (cf. *Carteria*) rather than the *Chlamydomonad*-type biflagellate which is considered basal to more advanced *Volvocales* [77, 78]. In the evolution of green algae, changes in the basal ultrastructure are thus major events [40] with the quadriflagellate condition arising multiple times. Three of the four *Pyramimonas* species considered here (*P. tetrahyinchus*, *P. octopus*, *P. cyrtoptera*) are assigned to the same subgenus according to morphological characters [79], and later by cladistic analysis of *rbcL* gene sequences confirming accelerated rates of evolution in this subgenus (Fig. 8). In these *Pyramimonas* species bearing 4, 8 or 16 flagella, ultrastructural modifications coincident with multiplicity and doubling of BBs may have evolved to enable strong coupling between opposite flagella pairs.

Latterly, the derivation of colonial volvocales from their unicellular ancestors enabled novel opportunities for flagellar coordination such as metachronism, but also imposes new constraints on their configuration and motion. Typically for colonial algae

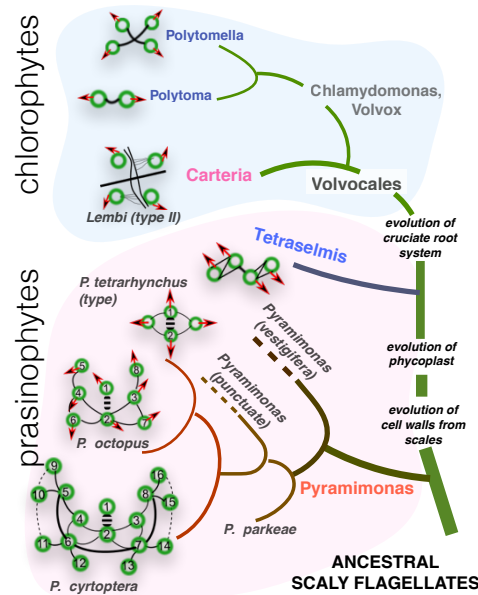


FIG. 8. Evolution of volvocales from ancestral scaly flagellates. Diagram shows species phylogeny, the geometric arrangement of their basal apparatuses, select fibrillar structures linking BBs, and (where known) the orientation of beating power strokes of attaching flagella.

such as VC, BBs reorient during early stages of development from the V-shape to a parallel configuration (recall Fig. 1C&D), and yet biflagellate VC sperm cells retain the V-formation. Even in ciliary arrays, structural modifications including ciliary roots and basal feet appear necessary for robust coordination for instance in mammalian cilia [80].

**Implications for active control of flagellar coordination.** In their lengthy evolution, the green algae display such extraordinary diversity of shape, geometry, symmetry and complexity of flagellar insertion, and yet the flagellar apparatus exhibits many derived characters that are traceable to common ancestry. Changes in cellular structure that are of fundamental evolutionary interest may thus have occurred in green flagellates rather than higher organisms. The diversity of multiflagellate gaits, and within a given algal species the capacity for selective activation of sub-groups of flagella, together suggests an inherent mechanism for pattern generation that may be conducted through contractile BB-associated fibers and rootlets.

The latter form a diverse, interconnecting network which is not only responsible for anchorage of apically inserted flagella, organellar placement, but which must now also be implicated in defining precise patterns of flagellar coordination. Indeed a direct correlation between cellular physiology and flagellar beating has been identified in CR [26]. When multiple flagella are positioned in close proximity, elastic forces between BBs can force nearest neighbours into modes of synchrony (IP or AP) that oppose the tendencies of hydrodynamic influences [15, 81]. The rapidity with which patterns of synchrony can change is suggestive of transduction by electrical signals or ionic currents [82], which may be effected from cell interior to flagella by changes in the state of contraction or relaxation of connecting fibers – where striations of algal rhizoplasts and fibers are biochemically mutable in a manner reminiscent of mammalian muscle. We are led to suggest that a parallel evolution of neuromuscular control of appendages may have occurred earlier than previously thought [50, 83].

## VI. MATERIALS AND METHODS

### A. Culturing and growth of algae

Below are brief descriptions of the protocols for species whose flagellar dynamics are studied here.

*Volvox*. *V. carteri* was prepared as described elsewhere [12]. The remaining species, unless otherwise specified, were maintained under controlled illumination on 14 : 10 day/night cycles, and at a constant temperature of 22°C (incubation chamber, Binder).

*Pyramimonas*. Marine species obtained from the Scandanavian Culture Collection of Algae and Protozoa, K-0006 *P. parkeae* R.E. Norris et B.R. Pearson 1975 (subgenus *Trichocystis*), K-0001 *P. octopus* Moestrup et Aa. Kristiansen 1987 (subgenus *Pyramimonas*), and K-0382 *P. cyrptoptera* Daugbjerg 1992 (subgenus *Pyramimonas*), were cultured in TL30 medium [84]. Of these, *P. cyrptoptera* is an Arctic species and was cultured at 4°C. A fourth *Pyramimonas*, K-0002 *P. tetrarhynchus* Schmarida 1850 (type species) is a freshwater species, and was grown in an enriched soil medium NF2 [84].

*Tetraselmis*. Marine species *T. suecica* (gift from University of Cambridge Department of Plant Sciences) and *T. subcordiformis* (CCAP 116/1A), were cultured in the f/2 medium [85].

*Polytoma*. *P. uvella* Ehrenberg 1832 (CCAP 62/2A) was grown in polytoma medium (comprising 2% sodium acetate trihydrate, 1% yeast extract and 1% bacterial tryptone [85]).

*Polytomella*. Two species (CCAP 63/1 and CCAP 63/3) were maintained on a biphasic soil/water medium [85].

*Carteria*. *C. crucifera* Korschikov ex Pascher (1927) from CCAP (8/7C) was grown in a modified Bold basal medium [85].

*Chlamydomonas*. *C. reinhardtii* strains were obtained from the Chlamydomonas Collection, wildtype CC125, and variable flagella mutant *vfl3* (CC1686), and grown photoautotrophically in liquid culture (Tris-Acetate Phosphate).

*Production of quadriflagellate dikaryons*. High-mating efficiency strains of *C. reinhardtii* CC620 (mt<sup>+</sup>), CC621 (mt<sup>-</sup>) were obtained from the Chlamydomonas Collection, and grown photoautotrophically in nitrogen-free TAP to induce formation of motile gametic cells of both mating types. Fusing of gametes occurred under constant white light illumination.

## B. Manipulation of viscosity

To facilitate identification of flagella in certain species, the viscosity of the medium was increased by addition of Methyl cellulose (M7027, Sigma Aldrich, 15 cP) to slow down cell rotation and translation rates.

## C. Microscopy and micromanipulation

The capture of single cells are as described elsewhere [12, 14, 16, 26]. For Fig. 3A caught CR cells were examined under the light microscope to identify the eyespot and thus *cis* and *trans* flagella; the correct flagellum was then carefully removed using a second pipette with smaller inner diameter.

## ACKNOWLEDGMENTS

This work is supported by a Junior Research Fellowship from Magdalene College Cambridge (KYW) and a Wellcome Trust Senior Investigator Award (REG). We thank Kyriacos Leptos and Marco Polin for discussions relating to the contractility of the basal apparatus at an early stage of this work, and the possible insights provided by the *vfl* class of mutants, François Peaudecerf for kindly providing the CR gametes, and Stephanie Höhn for valuable comments on the manuscript.

- 
- [1] H. Machemer, *Journal of Experimental Biology* **57**, 239 (1972).
  - [2] R. E. Goldstein, *Annual Review of Fluid Mechanics* **47**, 343 (2015).
  - [3] B. A. A. Orme, S. R. Otto, and J. R. Blake, *IMA Journal of Mathematics Applied in Medicine and Biology* **18**, 293 (2001).
  - [4] A. G. Kramer-Zucker, F. Olale, C. J. Haycraft, B. K. Yoder, A. F. Schier, and I. A. Drummond, *Development* **132**, 1907 (2005).
  - [5] B. Guirao and J. F. Joanny, *Biophysical Journal* **92**, 1900 (2007).
  - [6] K.-F. Lehtreck, M. J. Sanderson, and G. B. Witman, *Cilia: Structure and Motility* **91**, 255 (2009).
  - [7] D. J. Smith, E. A. Gaffney, and J. R. Blake, *Respiratory Physiology & Neurobiology* **163**, 178 (2008).
  - [8] J. Gray, *Ciliary Movement* (Cambridge University Press, 1928).
  - [9] Rothschild, *Nature* **163**, 358 (1949).
  - [10] I. H. Riedel, K. Kruse, and J. Howard, *Science* **309**, 300 (2005).
  - [11] S. Gueron and K. Levit-Gurevich, *Proceedings of the National Academy of Sciences of the United States of America* **96**, 12240 (1999).
  - [12] D. R. Brumley, K. Y. Wan, M. Polin, and R. E. Goldstein, *elife* **3**, e02750 (2014).
  - [13] C. A. Solari, K. Drescher, S. Ganguly, J. O. Kessler, R. E. Michod, and R. E. Goldstein, *Journal of the Royal Society Interface* **8**, 1409 (2011).
  - [14] D. R. Brumley, M. Polin, T. J. Pedley, and R. E. Goldstein, *Phys. Rev. Lett.* **109**, 268102 (2012).
  - [15] K. C. Leptos, K. Y. Wan, M. Polin, I. Tuval, A. Pesci, and R. E. Goldstein, *Phys. Rev. Lett.* **111**, 158101 (2013).
  - [16] K. Y. Wan, K. C. Leptos, and R. E. Goldstein, *Journal of the Royal Society Interface* **11**, 20131160 (2014).
  - [17] C. Huygens, *Horologium Oscillatorium, sive, De motu pendulorum ad horologia aptato demonstrationes geometricae* (F. Muguet., 1673).
  - [18] D. L. Ringo, *Journal of Cell Biology* **33**, 543 (1967).
  - [19] I. Inouye, *Ultrastructure of microalgae*, 99 (1993).
  - [20] K. Kunitomo, Y. Yamazaki, T. Nishida, K. Shinohara, H. Ishikawa, T. Hasegawa, T. Okanoue, H. Hamada, T. Noda, A. Tamura, S. Tsukita, and S. Tsukita, *Cell* **148**, 189 (2012).
  - [21] F. D. Galati, S. Bonney, Z. Kronenberg, C. Clarrisa, M. Yandell, and N. C. t. Elde, *Journal of Cell Biology* **207**, 705 (2014).
  - [22] G. I. Mcfadden, D. Schulze, B. Surek, J. L. Salisbury, and M. Melkonian, *Journal of Cell Biology* **105**, 903 (1987).

- [23] C. Carl, R. de Nys, R. J. Lawton, and N. A. Paul, *PLOS One* **9**, e97396 (2014).
- [24] F. A. Gilbert, *Mycologia* **19**, 277 (1927).
- [25] C. L. Dieckmann, *Bioessays* **25**, 410 (2003).
- [26] K. Y. Wan and R. E. Goldstein, *Physical Review Letters* **113**, 238103 (2014).
- [27] G. B. Witman, *Trends Cell Biology* **3**, 403 (1993).
- [28] R. E. Goldstein, M. Polin, and I. Tuval, *Physical Review Letters* **103**, 168103 (2009).
- [29] R. A. Lewin, *Biological Bulletin* **103**, 74 (1952).
- [30] R. L. Wright, B. Choknacki, and J. W. Jarvik, *Journal of Cell Biology* **96**, 1697 (1983).
- [31] R. L. Wright, J. L. Salisbury, and J. W. Jarvik, *Journal of Cell Biology* **101**, 1903 (1985).
- [32] S. Geimer and M. Melkonian, *Journal of Cell Science* **117**, 2663 (2004).
- [33] H. J. Hoops, R. L. Wright, J. W. Jarvik, and G. B. Witman, *Journal of Cell Biology* **98**, 818 (1984).
- [34] T. Niedermayer, B. Eckhardt, and P. Lenz, *Chaos* **18**, 037128 (2008).
- [35] J. S. Hyams and G. G. Borisy, *Journal of Cell Science* **33**, 235 (1978).
- [36] R. Kamiya and G. B. Witman, *Cell Motility and the Cytoskeleton* **98**, 97 (1984).
- [37] G. J. Elfring and E. Lauga, *Physical Review Letters* **103**, 088101 (2009).
- [38] K. D. Stewart and K. R. Mattox, *Biosystems* **10**, 145 (1978).
- [39] M. Melkonian, *Biosystems* **12**, 85 (1980).
- [40] D. Irvine and D. John, eds., *The Systematics Association special volume Systematics of the green algae*, Systematics Association, Vol. 27 (Academic Press, 1984).
- [41] C. J. O'Kelly and G. L. Floyd, *Biosystems* **16**, 227 (1983).
- [42] O. Moestrup and T. Hori, *Protoplasma* **148**, 41 (1989).
- [43] J. J. Collins and I. N. Stewart, *Journal of Nonlinear Science* **3**, 349 (1993).
- [44] G. Schoner, W. Y. Jiang, and J. A. S. Kelso, *Journal of Theoretical Biology* **142**, 359 (1990).
- [45] E. H. Harris, *The Chlamydomonas sourcebook. A comprehensive guide to biology and laboratory use.* (2009).
- [46] K. Y. Wan and R. E. Goldstein, "heterodynamic propulsion in flagellated algae," (2015).
- [47] D. R. Smith and R. W. Lee, *Plant Physiology* **164**, 1812 (2014).
- [48] I. Manton, *Proc. Linn. Soc. Lond* **179**, 147 (1968).
- [49] J. L. Salisbury, J. A. Swanson, G. L. Floyd, R. Hall, and N. J. Maihle, *Protoplasma* **107**, 1 (1981).
- [50] J. L. Salisbury and G. L. Floyd, *Science* **202**, 975 (1978).
- [51] S. D. Sym and R. N. Piernaar, *British Phycological Journal* **26**, 51 (1991).
- [52] W. Conrad, *Bulletin R. Hist. Nat. Belg.* **15**, 1 (1939).
- [53] P. Hargraves and W. Gardiner, *Journal of plankton research* **2**, 99 (1980).
- [54] T. Hori and O. Moestrup, *Protoplasma* **138**, 137 (1987).
- [55] N. Daugbjerg and O. Moestrup, *Canadian Journal of Botany-revue Canadienne De Botanique* **70**, 1259 (1992).
- [56] D. Sun, S. Roth, and M. J. Black, *International Journal of Computer Vision* **106**, 115 (2014).
- [57] N. Daugbjerg, O. Moestrup, and P. Archtander, *Journal of Phycology* **30**, 991 (1994).
- [58] V. F. Geyer, F. Jülicher, J. Howard, and B. M. Friedrich, *Proceedings of the National Academy of Sciences of the United States of America* **110**, 18058 (2013).
- [59] G. Quaranta, M. Aubin-Tam, and D. Tam, unpublished (2015).
- [60] N. Okita, N. Isogai, M. Hirono, R. Kamiya, and K. Yoshimura, *Journal of Cell Science* **118**, 529 (2005).
- [61] M. Bessen, R. B. Fay, and G. B. Witman, *Journal of Cell Biology* **86**, 446 (1980).
- [62] V. Mukundan, P. Sartori, V. F. Geyer, F. Jülicher, and J. Howard, *Biophysical Journal* **106**, 2434 (2014).
- [63] M. Melkonian, *Journal of Submicroscopic Cytology and Pathology* **15**, 121 (1983).
- [64] J. L. Salisbury, *Journal of Protozoology* **35**, 574 (1988).
- [65] I. R. Gibbons and A. V. Grimstone, *Journal of Biophysical and Biochemical Cytology* **7**, 697 (1960).
- [66] R. B. White and D. L. Brown, *Journal of Ultrastructure Research* **75**, 151 (1981).
- [67] M. Hayashi, T. Yagi, K. Yoshimura, and R. Kamiya, *Cell Motility and the Cytoskeleton* **41**, 49 (1998).
- [68] M. W. Watson, *Journal of Phycology* **11**, 439 (1975).
- [69] T. Matsusaka, *The Journal of cell biology* **33**, 203 (1967).
- [70] R. E. Norris and B. R. Pearson, *Archiv fuer Protistenkunde* **117**, 192 (1975).
- [71] D. L. Brown, A. Massalski, and R. Paternaude, *Journal of Cell Biology* **69**, 106 (1976).
- [72] C. A. Lembi, *Journal of Phycology* **11**, 1 (1975).
- [73] P. L. Beech, K. Heimann, and M. Melkonian, *Protoplasma* **164**, 23 (1991).
- [74] K. Hausman and R. Radek, eds., *Cilia and flagella, ciliates and Flagellates: ultrastructure and cell biology, function and systematics, symbiosis and biodiversity* (Schweizerbart Science Publishers, 2014).
- [75] T. Cavalier-Smith, *Biological Journal of the Linnean Society* **17**, 289 (1982).
- [76] F. Leliaert, D. R. Smith, H. Moreau, M. D. Herron, H. Verbruggen, C. F. Delwiche, and O. De Clerck, *Critical Reviews In Plant Sciences* **31**, 1 (2012).
- [77] M. A. Buchheim, C. Lemieux, C. Otis, R. R. Gutell, R. L. Chapman, and M. Turmel, *Molecular Phylogenetics and Evolution* **5**, 391 (1996).
- [78] H. Nozaki, O. Misumi, and T. Kuroiwa, *Molecular Phylogenetics and Evolution* **29**, 58 (2003).
- [79] G. I. Mcfadden, D. Hill, and R. Wetherbee, *Nordic Journal of Botany* **6**, 209 (1986).
- [80] E. R. Brooks and J. B. Wallingford, *Current Biology* **24**, R973 (2014).
- [81] M. Cosentino Lagomarsino, P. Jona, and B. Bassetti, *Physical Review E* **68**, 021908 (2003).

- [82] H. Harz and P. Hegemann, *Nature* **351**, 489 (1991).
- [83] G. Jékely, J. Paps, and C. Nielsen, *Evodevo* **6**, 1 (2015).
- [84] “<http://www.sccap.dk/media/>,” (2015).
- [85] “<http://www.ccap.ac.uk/pdfrecipes.htm>,” (2015).

## VII. SUPPLEMENTARY MATERIAL

We discuss here in more detail aspects of flagellar synchronization and swimming gaits in the unicellular green algae described in the text and SI Videos.

*Pairwise synchrony: tri-flagellated CR mutant.*

The *vfl3* mutant lacking or defective in distal striated fibers characteristically exhibits a variable number of flagella, each with apparently normal intrinsic motility but aberrant orientation. As a result, the flagella belonging to the same cell display greater frequency variance than the wildtype. When frequencies are sufficiently close, nearby configurations of flagella appear to be subject to significant hydrodynamic interactions. In the cell shown (Fig. S1) this leads to a competition between IP and AP components.

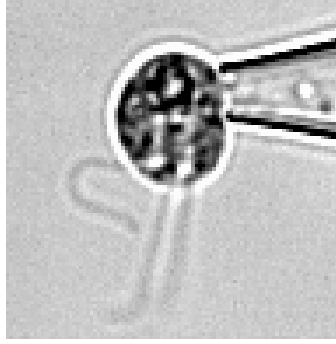


FIG. S1. Flagellar beating in the *vfl3* mutant. See also SI Video 1 and Fig. 2D. A cell with three flagella: the inner pair is oriented with power strokes in the same direction and tends towards IP synchrony, while the “outer” flagellum (leftmost) attempts to synchronize in antiphase with respect to the first pair.

*Pairwise synchrony: two VC somatic cells.* Here we elaborate on observed pairwise synchronization states between the flagella of two *V. carterii* somatic cells held in close proximity and with opposing power strokes, with particular emphasis on the consistency with theoretical predictions based on hydrodynamic interactions. As discussed in the main text, two states are observed (IP and AP), with the AP being preferred/more stable than the IP (Figs. 3 and S2). Transitions between IP and AP synchrony appear to be stochastic, stemming from inherent biochemical noise in the system. Within either state however, precise phase relationships are maintained. For interpolated flagellar phases  $\phi_{1,2}$  ( $\in [0, 2\pi]$ ) measured for each flagellum directly from the experimental data, we plot  $\cos(\phi_{1,2})$  in SI Videos 2&3.

It is convenient and insightful to consider a dimension-reduced model in which each flagellum is modelled as a sphere of radius  $a$  constrained to oscillate along a near-circular trajectory of radius  $R$  [4]. Let  $\hat{\mathbf{e}}_{\phi_i} = (-\sin(\phi_i), \cos(\phi_i))$  and  $\hat{\mathbf{e}}_{r_i} = (\cos(\phi_i), \sin(\phi_i))$  denote unit vectors in the tangential and radial directions for each flagellum  $n$ , and measure phases  $\phi_{1,2}$  CCW from the +ve x-axis. The two spheres are centered at  $\mathbf{r}_{01,2}$ , separated by  $\ell = |\mathbf{r}_{02} - \mathbf{r}_{01}|$  which is assumed large so that  $a \ll \ell$  and  $R \ll \ell$  (i.e. hydrodynamic far field), but simulations and experimental studies on colloidal systems have shown that qualitative predictions of the theory are still applicable even in situations where these values are not so small.

The velocities are given by  $\mathbf{u}_i = \dot{R}_i \hat{\mathbf{e}}_{r_i} + R_i \dot{\phi}_i \hat{\mathbf{e}}_{\phi_i}$ . The orbital radius is assumed to be flexible, characterized by a spring constant  $k$  and natural length  $R_0$ . Even for a simple driving force (assumed proportional to angular velocity), this flexibility allows each sphere to respond to hydrodynamic perturbations arising from the motion of its neighbor thereby leading to trajectory deformations of the correct sign to achieve synchronization. More generally, we can incorporate an additional variable driving force so that, for example,

$$\mathbf{F}_i = -k(R_i - R_0)\hat{\mathbf{e}}_{R_i} + F(\phi_i)\hat{\mathbf{e}}_{\phi_i},$$

where

$$F(\phi_i) = F_0(1 - A \sin(2\phi_i))$$

acting tangentially along the orbit [2]. Depending on orbital rigidity one or the other of the two contributions will dominate [6]. For rapid synchronization of flagella, it has been shown that orbital compliance dominates over force modulation [12]. For counter-rotating spheres, if we take  $F(\phi_1) = F_0(1 - A \sin(2\phi_1))$  then  $F(\phi_2) = -F_0(1 + A \sin(2\phi_2))$ .

Motion is described [1] by the force balance  $\mathbf{u}_i = \mathbf{O}_{ij}\mathbf{F}_j$ , where

$$\mathbf{O}_{ij} = \zeta^{-1} \left( \delta_{ij} + (1 - \delta_{ij}) \frac{3a}{4r_{ij}} \left( 1 + \frac{\hat{\mathbf{r}}_{ij}\hat{\mathbf{r}}_{ij}}{r_{ij}^2} \right) \right), \quad (i, j = 1, 2)$$

where  $\zeta = 6\pi\eta a$  is the drag coefficient of a sphere and  $\hat{\mathbf{r}}_{ij} = (\mathbf{r}_j - \mathbf{r}_i)/r_{ij} \simeq \hat{\mathbf{x}} + \mathcal{O}(R/\ell)$ . Force balance in the tangential and radial directions gives:

$$\begin{aligned} \zeta \dot{R}_i &= \epsilon \left( 1 + \hat{\mathbf{x}}\hat{\mathbf{x}} \right) \mathbf{F}_i \cdot \hat{\mathbf{e}}_{R_i} - k(R_i - R_0) \\ \zeta R_i \dot{\phi}_i &= F(\phi_i) + \epsilon \left( 1 + \hat{\mathbf{x}}\hat{\mathbf{x}} \right) \mathbf{F}_i \cdot \hat{\mathbf{e}}_{\phi_i}, \end{aligned} \quad (7)$$



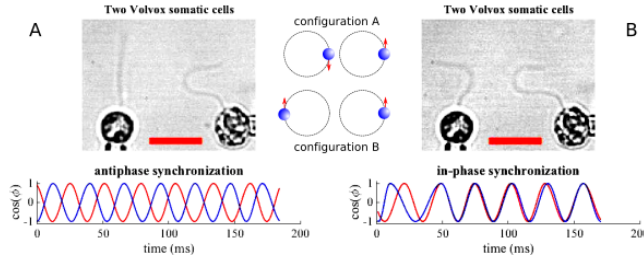


FIG. S2. Synchronization of flagella on *Volvox* somatic cells. As each flagellum is on a separate pipette-held cell, coupling is solely through the intervening fluid. The beating patterns correspond to configurations of counter-rotating spheres which tend to (A) AP or (B) IP states; state A is more stable and has a higher frequency than B, as predicted. See SI Videos 2&3. Scale bars are  $10 \mu\text{m}$ .

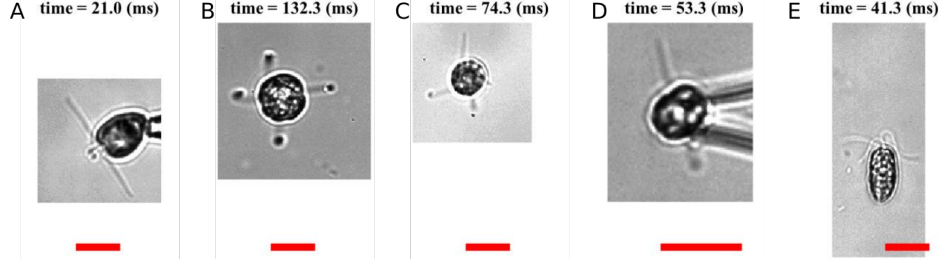


FIG. S3. Distinctive quadriflagellate gaits. See Fig. 4 of text and SI Video 4. (A) trot (*Pyramimonas parkeae*) held stationary by a micropipette, (B) pronk (*Pyramimonas tetrahynchus*), (C) rotary gallop of *Carteria crucifera* and of *Tetrasmis suecica* viewed apically when (D) held by micropipette or (E) freely-swimming. Scale bars are  $10 \mu\text{m}$ .

where  $\epsilon = 3a/4\ell$ . If radial variations decay much faster than tangential ones, so  $\dot{R} \simeq 0$ , then  $k(R_i - R_0) \sim \mathcal{O}(\epsilon)$ , and we can further expand  $\mathbf{F}_i/\zeta \approx R_i \dot{\phi}_i \hat{\mathbf{e}}_{\phi_i} + \mathcal{O}(\epsilon)$ . The dynamics of oscillator 1 is then given by

$$\begin{aligned} \zeta \dot{\phi}_1 = & F_1(\phi_1) + \frac{\epsilon F_i(\phi_i)}{2R_0} [3 \cos(\phi_1 - \phi_2) - \cos(\phi_1 + \phi_2)] \\ & - \frac{\epsilon F_i(\phi_i) F_j(\phi_j)}{2kR_0^2} [3 \sin(\phi_1 - \phi_2) - \sin(\phi_1 + \phi_2)], \end{aligned} \quad (8)$$

and similarly for oscillator 2 under interchange of  $1 \leftrightarrow 2$ .

For counter-rotating spheres the phase sum  $\Xi = \phi_1 + \phi_2$  fluctuates about  $\Xi_0 = 0$  or  $\Xi_0 = \pi$  in either AP or IP states. In the case of AP synchrony, let  $\Xi = \Xi_0 + \delta$ , then  $\phi_2 = \phi$ , and  $\phi_1 = \delta - \phi$ , and we have

$$\begin{aligned} \zeta \frac{\dot{\delta}}{\delta} \simeq & -2 \frac{F_0 A}{R_0} \cos(\phi) - \frac{\epsilon F_0 A}{R_0} \cos(2\phi) (3 \cos(2\phi) - 1) \\ & - \frac{\epsilon F_0^2}{kR_0^2} (1 + A \sin(2\phi))^2, \end{aligned}$$

and similarly for the IP state - for a change of sign to the last term in the above. This last term corresponds to elastic deformation of orbits, and is  $< 0$  (leading to stability) for all phases  $\phi$  in the case of AP synchronization but  $> 0$  (leading to instability) in the case of IP synchronization, consistent with our experimental observations. Furthermore the average period  $T_{\text{AP,IP}}$  of these metastable states is then given by  $\int_0^{2\pi} \dot{\phi}^{-1} d\phi$  [3]:

$$T_{\text{AP,IP}} = \frac{2\pi \zeta R_0}{F \sqrt{1 - A^2}} \left( 1 \mp \frac{1}{2} \epsilon \right). \quad (9)$$

From the data, we find the experimental configuration to be consistent with  $a \simeq 3 \mu\text{m}$  for a separation of  $\ell \simeq 15 \mu\text{m}$ ; in particular, the AP state is indeed faster than the IP.

*Swimming with four flagella.* Select species of quadriflagellates exemplify the possible gait symmetries. The motion is highly species-specific, where the patterns or sequence of actuation of the flagella appear to be independent of whether or not the cell body has been fixed in place.

*Flagellar synchronization in a dikaryon of Chlamydomonas.* Although CR is most likely to occur in its vegetative state, gametic cells capable of sexual reproduction can form under nitrogen deprivation in the presence of light. When two biflagellate CR gametes of opposite mating types (+ and -) come together, flagellar agglutination [8] occurs whereby the flagella of opposite mating types adhere strongly to each other (Figure. S4A1). This is followed by autolysin secretion which digests away the cell walls, after which a fertilization tubule extends from the + gamete to its partner (Figure. S4A2). If fusion is successful, a single temporary dikaryon is formed, which is quadriflagellate (Figure. S4A3).

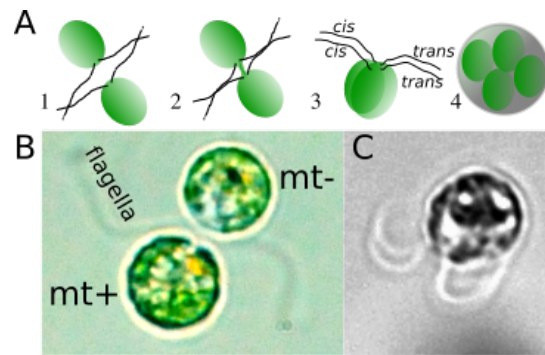


FIG. S4. Generation of a dikaryon of *Chlamydomonas*. For brevity, eyespot locations are not shown. (A) 1-4: Life cycle of sexual reproduction in CR. (B) A pair mating (stage 1). (C) A quadriflagellate dikaryon is formed. See SI Video 5.

These dikaryons exhibit a striking double bilateral breaststroke (in contrast to the double cruciate breaststroke observed in *P. parkeae*), in which pairs of flagella on the same side become strongly phase-synchronized. It is known that the flagella separate distally into *cis-cis* and *trans-trans* pairs, allowing cells to remain strongly phototactic during this period, which is another indication of good flagellar coordination. Eventually, maturation of the zygotes leads to resorption of all flagella, and formation of a CR spore. These diploid zygotes await favorable conditions before release of 4 new haploid progeny.

*Swimming with eight flagella.* The octoflagellate *P. octopus* displays stochastic switching between a number of different gaits (Fig. S5 and SI Video 6). Primary among these is a complex breaststroke which appears to involve a number of phase-shifted pairwise IP breaststrokes. The IP synchrony within certain of the pairs are more robust than in others (the basal architecture is far from radially symmetric, with the large synistosome connecting BB1 and 2 (see Fig. 8).

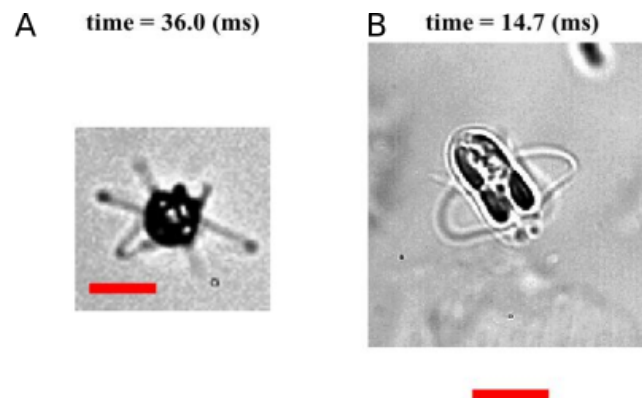


FIG. S5. Swimming dynamics of the octoflagellate *P. octopus*. (A) View from the top, where the cell is observed to rotate CCW about its long axis over time, and (B) view from the side, where several pairs of in-phase breaststrokes are observed, principally between diametrically opposed flagella. See SI Video 6. Scale bars are 10  $\mu\text{m}$ .

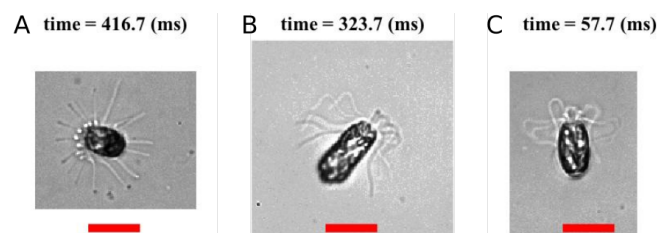


FIG. S6. Distinctive hexadecaflagellate gaits. (A) Pronk: all flagella synchronized (a hydrodynamic mode). (B) bilateral: one group comprising half of the flagella are synchronized, but are in anti-phase relative to the complementary group. (C) mixed mode: resembles a *P. octopus*. See SI Video 7. Scale bars are 20  $\mu\text{m}$ .

*Swimming with sixteen flagella.* Flagellar coordination in the hexadecaflagellate *P. cyrtoptera* leads to a number of distinctive gaits which may be dependent on the current state of contractile of the fiber network: three of which are shown here (Fig. S6 and SI Video 7). (A) Significant

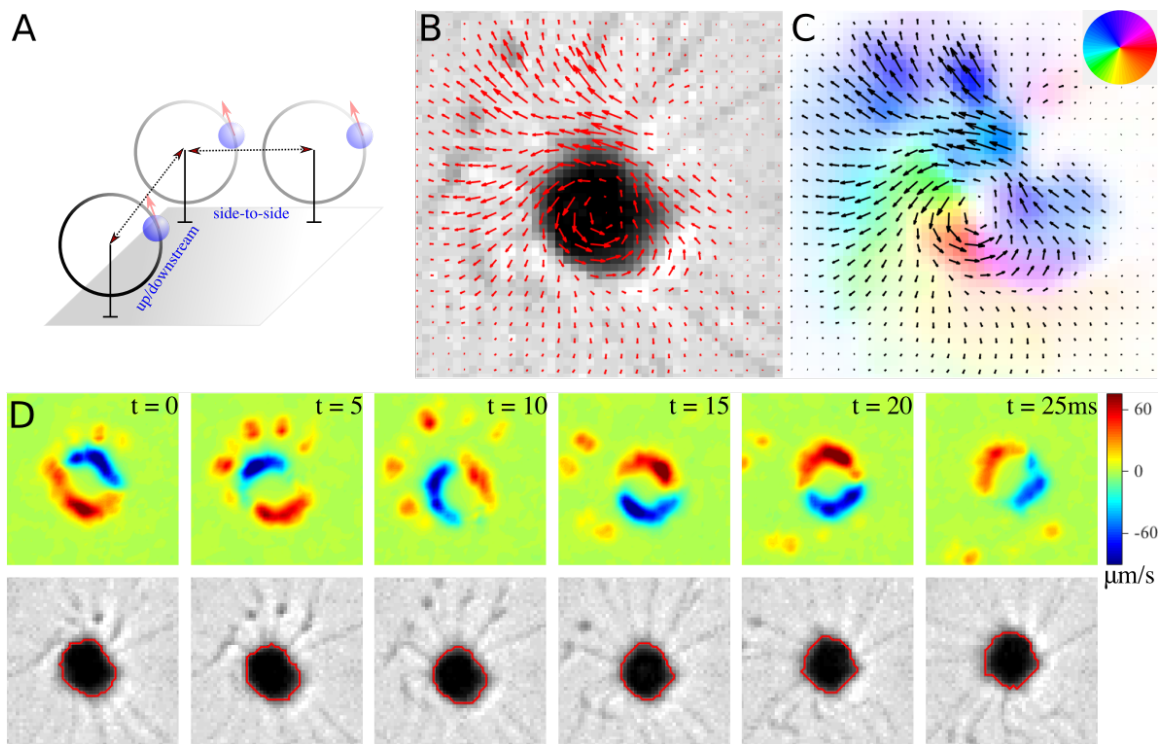


FIG. S7. Metachronism in a hexadecaflagellate. (A) The strength of hydrodynamic interactions between pairs of flagella is strongly dependent on their relative orientation. This leads to the formation of symplectic metachronal waves in a finite ring of flagellar oscillators, representing the hexadecaflagellate. (B,C) The average (optical) flow field  $\langle \bar{U} \rangle$  around *P. cyrtoptera*. (D) Snapshots of the radial components of optical flow field.

nearest-neighbour hydrodynamic effects can synchronize all sixteen flagella, which prongs with a well defined periodicity coinciding with the beat frequency of an individual flagellum. (B) The underlying basal-body network exhibits significant bilateral symmetry (Fig. 8), which could explain the frequent appearance of a bilateral gait in which flagella are divisible into two groups, which beat alternately. Flagella within each group appear to be strongly coupled in IP by hydrodynamic interactions. As a result the cell body sways periodically from side to side. (C) In certain individuals, basal coupling appears strong enough to permit several phase-shifted breaststroke pairs and swimming is reminiscent of an octoflagellate with flagella doubled up in pairs - with the flagella in each pair undulating in perfect unison.

#### *Emergence of metachronism in a hexadecaflagellate*

In *P. cyrtoptera*, neighboring flagella experience strong hydrodynamic interactions due to their close spatial proximity, giving rise to the striking pronging gait (SI Video 7) in which all sixteen flagella beat with zero relative phase difference. In this organism yet another phenomenon can be attributed to hydrodynamic synchronization: occasionally, we observe metachronal waves propagating circumferentially around the crown of flagella which become especially notable in cells swimming close to surfaces. We discuss below how this is consistent with theory concerning fluid-structure interactions near no-slip surfaces, and where dynamics are dominated by orbital compliance (Fig. S7).

Firstly, steric interactions near the wall forces the flagella to ‘flatten’ or reorient more laterally, contrary to the normal state in which they are recurved longitudinally along the cell body from the anterior to the posterior. This new orientation becomes more conducive to hydrodynamic coupling [14] between the flagella (Fig. S7A). Interactions are maximised when flagella are placed side-by-side and minimized when placed in the up/downstream directions. Secondly, proximity near the no-slip boundary itself means that the nearest-neighbor contribution to the coupling is increased, again encouraging the emergence of metachronal waves.

For the cell shown, a symplectic metachronal wave propagates CCW among its flagella, which causes the cell to rotate very slowly in a CW sense. We take the optical flow field  $\mathbf{U}(\mathbf{r}; t)$  as proxy for the real flow field in the vicinity of the organism (there is good agreement in direction even if flow magnitudes are less reliable). The time averaged flow field (Fig. S7) is clearly rotary

$$\langle \mathbf{U}(\mathbf{r}; t) \rangle = \frac{1}{t} \int_0^t \mathbf{U}(\mathbf{r}; t) dt$$

We decompose the flow into its radial and tangential components  $\mathbf{U}(\mathbf{r}; t) = U_r(\mathbf{r}; t)\mathbf{e}_r + U_\theta(\mathbf{r}; t)\mathbf{e}_\theta$ , and concentrate on the radial component which corresponds the direction perpendicular to the wall, since forces perpendicular to a wall decay much faster than the tangential contribution. The plots reproduce features distinctive of a metachronal wave.

- 
- [1] Happel J, Brenner H (1983) Low Reynolds number hydrodynamics: with special applications to particulate media. *Kluwer, New York*
- [2] Uchida G, Golestanian (2012) Hydrodynamic synchronization between objects with cyclic rigid trajectories. *The European Physical Journal E* 35: 1-14
- [3] Box S, Debono L, Philips DB, Simpson SH (2015) Transitional behavior in hydrodynamically coupled oscillators. *Phys. Rev. E* 91 (022916)
- [4] Niedermayer T, Eckhardt B, Lenz P (2008) Synchronization, phase locking and metachronal wave formation in ciliary chains. *Chaos* 18(037128)
- [5] Bruot N, Kotar J, de Lillo F, Cosentino Lagomarsino M, Cicuta P (2012) Driving potential and noise level determine the synchronization state of hydrodynamically coupled oscillators *Phys. Rev. Lett* 109 (164103)
- [6] Kotar J, Debono L, Bruot N, Box S, Philips DB, Simpson SH, Hanna S, Cicuta P (2013) Optimal hydrodynamic synchronization of colloidal oscillators. *Phys. Rev. Lett* 111 (228103)
- [7] Brumley DR, Polin M, Pedley TJ, Goldstein RE (2012) Hydrodynamic synchronization and metachronal waves on the surface of the colonial alga *Volvox carteri*. *Phys. Rev. Lett* 109 (268102)
- [8] Harris EH (2009) The *Chlamydomonas* Sourcebook: Introduction to Chlamydomonas and its laboratory use, *Academic Press, Oxford, England*
- [9] Holmes JA, Dutcher SK (1989) Cellular asymmetry in *Chlamydomonas reinhardtii*, *Journal of Cell Science* 94: 273–285